Impact of the neutron-star deformability on equation of state parameters

C. Y. Tsang, M. B. Tsang, Pawel Danielewicz, and W. G. Lynch
National Superconducting Cyclotron Laboratory and the Department of Physics and Astronomy, Michigan State University, East Lansing, Michigan 48824, USA

F. J. Fattoyev
Department of Physics, Manhattan College, Riverdale, New York 10471, USA

(Received 14 January 2020; revised 1 April 2020; accepted 22 September 2020; published 19 October 2020)

We use a Bayesian inference analysis to explore the sensitivity of Taylor expansion parameters of the nuclear equation of state (EOS) to the neutron star dimensionless tidal deformability (Λ) on 1- to 2-solar-mass neutron stars. A global power law dependence between tidal deformability and the compactness parameter (M/R) is verified over this mass region. To avoid superfluous correlations between the expansion parameters, we use a correlation-free EOS model based on a recently published metamodeling approach. We find that assumptions in the prior distribution strongly influence the constraints on Λ. The Λ constraints obtained from the neutron star merger event GW170817 prefer low values of $L_{\rm sym}$ and $K_{\rm sym}$, for a canonical neutron star with 1.4 solar masses. For a neutron star with mass $<$1.6 solar masses, $L_{\rm sym}$ and $K_{\rm sym}$ are highly correlated with the tidal deformability. For more massive neutron stars, the tidal deformability is more strongly correlated with higher order Taylor expansion parameters.

DOI: 10.1103/PhysRevC.102.045808

I. INTRODUCTION

A neutron star (NS) is the remnant of a supernova explosion of a massive star. The interior of a NS contains the densest nuclear material in the universe. This matter is so dense that it becomes energetically favorable for protons and electrons to combine and form neutrons. From densities ranging from somewhat below saturation density ($\rho_0 = 0.155\,\mathrm{fm}^{-1}$) to $3\rho_0$, it is reasonable to describe NS matter as locally uniform nuclear matter composed mostly of neutrons. Study of NSs is of great relevance to nuclear physics because of the information it can provide regarding the equation of state (EOS) of asymmetric nuclear matter at high density. Even though the current paper is self-contained with relevant materials detailed in Appendixes and extensive references, for those who are interested, Refs. [1–4] provide more in depth discussions of the subjects.

Astrophysical NS properties, combined with constraints from nuclear observations, have provided a rough understanding of the EOS. Typical temperatures of NSs are low, $k_BT <$ 1 MeV; thus the finite temperature effect is small and the main uncertainties in the EOS concern the relation between the pressure and energy density of nuclear matter at various baryon densities [5].

Measurements of collective flow and kaon production in energetic nucleus-nucleus collisions have constrained the EOS for symmetric matter, at densities up to $4.5\rho_0$ [6–8]. Specifically, the symmetric matter constraints on pressure vs density were determined in Ref. [6] from the measurements of transverse and elliptical flow from Au + Au collisions over a range of incident energies from 0.3 to 1.2 GeV/nucleon. More recently, these constraints were confirmed in an independent analysis of elliptical flow data [9]. In Refs. [7,8], a similar constraint from $1.2\rho_0$ to $2.2\rho_0$ was obtained from the kaon measurements. These heavy ion constraints are consistent with the Bayesian analyses of the neutron-star mass-radius correlation in Ref. [10].

Recent gravitational wave observations from the LIGO Collaboration [11] opened a new window for understanding neutron-star matter. Specifically, the LIGO observation provides estimates for the tidal deformability, also known as tidal polarizability, a quantity that bears direct relevance to the nuclear EOS.

The tidal deformability is induced when two NSs orbit around each other and tidal forces from each NS deforms its companion star. The mass quadrupole that developed in response to the external quadrupole gravitational field emerges as

$$Q_{ij} = -\lambda E_{ij}. \tag{1}$$

Here E_{ij} is the external gravitational field strength and λ is the tidal deformability. The orbital period of the inspiral differs from that of two point masses because the additional tidal deformation contributes to an overall orbital energy loss and changes the rotational phase. This difference is used to extract the dimensionless tidal deformability (Λ) of a NS [12,13]. Throughout this paper, tidal deformability given below always refers to the dimensionless tidal deformability,

$$\Lambda = \frac{\lambda c^{10}}{G^4 M^5} = \frac{2}{3} k_2 \left(\frac{c^2 R}{GM}\right)^5, \tag{2}$$

where k_2 is the second Love number [14,15]. This whole expression, including the Love number, is sensitive to the nuclear EOS [11,16,17]. Steps necessary to calculate Λ for a given EOS are detailed in Appendix A. Recent analysis of the gravitational wave data constrained this value to $\Lambda = 190^{+390}_{-120}$ [18].

Since most observables from nuclear structure experiments constrain the energy density and its derivatives near or somewhat below saturation density (see, for example, Refs. [19–22]), it is customary to approximate the EOS by a Taylor expansion about saturation density. We explore the parameter space spanned by the derivatives of the EOS with respect to density at ρ_0 and examine its correlation with Λ.

Other studies have been carried out in placing tidal deformability constraints on these Taylor expansion parameters. They explored the constraints on different two-dimensional parameter planes [21,23], on a diverse set of models [24–26], and with Bayesian analysis on EOSs from chiral effective field theory [27]. In this study, we expand the analysis by employing a less restrictive form of EOS and exploring a larger parameter space by including higher order terms.

A family of theoretical EOSs is needed to correlate the Taylor expansion parameters with the predicted Λ. One widely used family in astrophysics is the piecewise polytropes [28], but it is not suitable in this study because a Taylor expansion assumes that the EOS is analytic over the range of interest. As long as there is only one polytrope, a Taylor expansion is valid, but its validity does not extend past the point of connection between the original polytrope and the next.

Another commonly used family is the Skyrme-type EOS [29]. It derives from simplified approximate nuclear interaction and relies on 15 free parameters in its expanded form. While it is shown to successfully reproduce various nuclear properties, it is difficult to explore new physics from the Taylor expansion parameters because they are strongly constrained by the form of the Skyrme interaction itself. With the functional form of Skyrme EOS, different Taylor expansion parameters may not be independent of each other [30,31].

In this study, an EOS from metamodeling [32] is used. By construction, their derivatives of different orders are independent of each other. This paper is organized as follows: In Sec. II, a brief description of Bayesian inference is provided. This is the statistical method employed in the extraction of EOS information from NS tidal deformability constraints. Section III describes our choice of EOS from the metamodeling approach in Ref. [32] and how it is adopted to describe a neutron star. In Sec. IV, correlation between EOS parameters and tidal deformability of a 1.4-solar-mass NS is discussed. Section V extends the study to NSs of different masses and Sec. VI summarizes our findings.

II. BAYESIAN INFERENCE

We use Bayesian inference to study the influence of tidal deformability constraints from LIGO on nuclear-matter EOS parameters. These parameters are sampled with a prior probability distribution based on findings from literature and are then transformed into a distribution of neutron-star matter EOSs. Through solving the Tolman-Oppenheimer-Volkoff (TOV) equation, we are able to calculate the corresponding tidal deformabilities. By combining their prior distribution and likelihood, which indicates the compatibility between the calculated and the observed tidal deformability, Bayesian inference will assign probability for each EOS parameter with Bayes's theorem:

$$P(\mathcal{M}) = \frac{1}{V_{\rm tot}} w(\mathcal{M}) p(\Lambda(\mathcal{M})) \prod_i g_i(m_i). \tag{3}$$

In this equation, $\mathcal{M}$ is the set of all EOS parameters, $m_i \in \mathcal{M}$ is one of the EOS parameters, $V_{\rm tot}$ is the feature scaling constant, $p(\Lambda(\mathcal{M}))$ is the likelihood of an EOS calculated from its predicted Λ, g_i is the prior distribution of the ith parameter, and $w(\mathcal{M})$ is the filter condition that filters out EOS parameter space that is nonphysical.

The likelihood of the EOS is the probability of having the observed LIGO event with the assumption that the given theoretical EOS is the ultimate true EOS. We model the likelihood function as an asymmetric Gaussian distribution base on the extracted $\Lambda = 190^{+390}_{-120}$ [18] from GW170817:

$$p(\Lambda) = \begin{cases} \frac{1}{V} \exp\left(-\frac{(\Lambda-190)^2}{2\times 120^2}\right) & \text{if } \Lambda \leqslant 190 \\ \frac{1}{V} \exp\left(-\frac{(\Lambda-190)^2}{2\times 390^2}\right) & \text{if } \Lambda > 190. \end{cases} \tag{4}$$

In the above, V is the feature scaling constant such that the likelihood function integrates to 1.

The sought function is the probability distribution of EOS parameters rather than that for Λ, so prior distribution g_i is required to convert between the two using Bayes's theorem. A commonly used prior is the Gaussian distribution:

$$g_i(m_i) = \frac{1}{\sqrt{2\pi\sigma_i^2}} \exp\left(-\frac{(m_i - m_{i,\rm prior})^2}{2\sigma_i^2}\right), \tag{5}$$

where $m_{i,\rm prior}$ and σ_i are the prior mean and standard deviation of the free parameters, respectively. They should be chosen to reflect our current understanding of those free parameters.

Some parameter sets may yield nonphysical EOSs due to various additional considerations. The filter condition $w(\mathcal{M})$ takes that into account; it is set to 1 if the following three conditions of stability, causality, and maximum mass are all satisfied, and it is set to zero if not.

The stability condition rejects EOSs whose pressure decreases with energy density. Above the crust-core transition density, we require the EOSs to be mechanically stable with thermodynamical compressibility greater than zero, which means that the pressure of homogeneous matter does not decrease with density. For EOSs with negative compressibilities at density above the crust-core transition densities predicted by Eq. (15), they will be rejected as being inconsistent with experimental information.

The requirement of causality rejects EOSs whose speed of sound is greater than the speed of light in the core region of their respective heaviest NS. The maximum mass condition rejects EOSs that fail to produce a NS of at least 2.04 solar masses in accordance with observation [33,34].

Using the fact that the binary NS merger GW170817 detected by LIGO did not promptly produce a black hole, Ref. [35] inferred that the heaviest possible NS should be

around 2.17 solar masses. Other sources put the maximum mass at around 2.15–2.40 solar masses [36–41]. Neither of these constraints has been adopted in this work but can be implemented in the future.

The calculated probability distribution from Eq. (3) is referred to as the posterior distribution. By comparing prior to posterior distribution, we are able to infer the sensitivity of various EOS parameters to NS tidal deformability. By construction, priors of different free parameters in metamodeling the EOS are not correlated with each other, so any correlations in the posterior reflect the collective sensitivity of the Taylor expansion parameters to NS tidal deformability.

III. NUCLEAR EQUATION OF STATE

A. Parameters in nuclear EOS

Nuclear matter is a theoretical construct composed of protons and neutrons. It resembles the core of ordinary nuclei where the neutron and proton densities are approximately uniform. Since the numbers of protons and neutrons are usually not far from each other in nuclei, we often expand the EOS into the symmetric nuclear matter (SNM) term (isoscalar term) and a correction term for the deviation from SNM (isovector term), when proton densities and neutron densities are not identical as shown in Eq. (6) below. SNM refers to an infinite system where the density of protons equals the density of neutrons. The EOS is commonly expanded as

$$E(\rho,\delta) = E_{is}(\rho) + \delta^2 E_{iv}(\rho). \tag{6}$$

In the above, E_{is} is the isoscalar term, E_{iv} is the isovector term, ρ is the matter density, and $\delta = (\rho_n - \rho_p)/(\rho_n + \rho_p)$ is called the asymmetry parameter where ρ_n and ρ_p are neutron density and proton density respectively. Nuclear structure probes are generally sensitive to the density region around saturation (ρ_0) [19–22] and, as a result, derivatives of the EOS with respect to density at this point are often used as empirical parameters to characterize the density and isospin dependence of the EOS. The derivatives are commonly expressed as parameters in the Taylor expansion when the EOS is expanded in terms of $x = (\rho - \rho_0)/(3\rho_0)$:

$$E_{is}(\rho) = E_0 + \frac{1}{2}K_{\rm sat}x^2 + \frac{1}{3!}Q_{\rm sat}x^3 + \frac{1}{4!}Z_{\rm sat}x^4 + \cdots, \tag{7}$$

$$E_{iv}(\rho) = S_0 + L_{\rm sym} + \frac{1}{2}K_{\rm sym}x^2 + \frac{1}{3!}Q_{\rm sym}x^3 + \frac{1}{4!}Z_{\rm sym}x^4 + \cdots. \tag{8}$$

One focus of this paper is to explore the sensitivity between Λ and S, L, K, Q, and Z. Some families of EOSs depend on density and asymmetry in a way that cannot be separated explicitly into the sum of two terms, but the isoscalar term is always well defined:

$$E_{is}(\rho) = E(\rho, \delta = 0). \tag{9}$$

The isovector term can be defined as the second order Taylor expansion coefficient in δ around $\delta = 0$ (not to be confused with Taylor EOS expansion parameters, which expand in x),

$$E_{iv}(\rho) = \frac{1}{2}\frac{\partial^2 E(\rho,\delta)}{\partial\delta^2}\Big|_{\delta=0}. \tag{10}$$

Likewise Taylor EOS parameters can always be extracted from any nuclear EOS. This allows for comparison of variables across families of EOSs.

Another important quantity that characterizes nuclear matter properties is the effective mass $m^*(\rho,\delta)$. It is used to characterize the momentum dependence of nuclear interaction and it can be different for protons, $m^*_{\rm p}(\rho,\delta)$, and neutrons, $m^*_{\rm n}(\rho,\delta)$, depending on the condition which the nuclear matter is subjected to. It is generally assumed that $m^*_{\rm p} = m^*_{\rm n}$ in SNM.

Comparison of effective mass is commonly carried out through the comparison of two quantities: the nuclear effective mass in SNM at saturation, $m^*_{\rm sat}$, and the splitting in neutron and proton effective masses in pure neutron matter (PNM) at saturation, $\Delta m^* = m^*_{\rm n} - m^*_{\rm p}$. The choice of the two quantities mirrors the spirit of splitting the EOS into an isoscalar term and an isovector term in Eq. (6) in which contribution from SNM is separated from the correction factor that arises when matter is not symmetric.

Sometimes it is more convenient to express $m^*_{\rm sat}$ and Δm^* in terms of $\kappa_{\rm sat}$, $\kappa_{\rm sym}$, and κ_v:

$$\kappa_{\rm sat} = \frac{m}{m^*_{\rm sat}} - 1 = \kappa_s,$$
$$\kappa_{\rm sym} = \frac{1}{2}\left(\frac{m}{m^*_n} - \frac{m}{m^*_p}\right),$$
$$\kappa_v = \kappa_{\rm sat} - \kappa_{\rm sym}. \tag{11}$$

The parameter κ_v plays the role of the enhancement factor in the Thomas-Reiche-Khun sum rule and it depends on the energy region of the resonance energy [42]. In this analysis, the effective masses are expressed in terms of $m^*_{\rm sat}/m$ and κ_v.

B. EOS from a metamodeling approach

Our studies utilizing the metamodeling analysis follow the approach of Ref. [32]. Such metamodels for the EOS can be easily constructed with only Taylor expansion parameters and effective masses. The metamodel EOS resembles the Skyrme EOS with the same corresponding Taylor parameters to a greater extent than a simple power law expansion.

Four different empirical local density functional (ELF) metamodels are proposed in Ref. [32]: ELFa, ELFb, ELFc and ELFd. ELFa does not produce vanishing energy as density approaches zero. ELFb does not converge to a typical Skyrme EOS even when identical Taylor parameters are used. ELFc does not have the shortcomings of EFLa and ELFb and closely resembles the Skyrme with similar Taylor parameters. Although ELFd agrees with Skyrme better, it relies on high density information that is not well constrained by experiments.

From the above considerations, we adopt ELFc in this study. A similar choice is also made in other recent studies [43,44]. The formulation of ELFc is detailed in Appendix B. As assessed in Ref. [32], the following choices of parameters have been accurately constrained by nuclear experiment

and are fixed in the analysis: $E_{\rm sat} = -15.8\,{\rm MeV}$ and $\rho_0 = 0.155\,{\rm fm}^{-3}$.

C. Thermodynamic relations

Additional characteristics of nuclear matter can be inferred using thermodynamic equations once an EOS is specified. The pressure at various densities, $P(\rho)$, is related to the derivative of the energy:

$$P(\rho) = \rho^2 \frac{\partial E(\rho,\delta)}{\partial \rho}. \tag{12}$$

The adiabatic speed of sound can then be calculated [45]:

$$\left(\frac{v_s}{c}\right)^2 = \left(\frac{\partial P}{\partial \mathcal{E}}\right)_S, \tag{13}$$

where $\mathcal{E} = \rho(E + mc^2)$ is the energy density of the material including mass density. This implies any thermodynamic stable EOS must satisfy $(\frac{\partial P}{\partial \mathcal{E}})_S > 0$. Furthermore, since information cannot travel faster than the speed of light due to causality, the inequality $v_s < c$ must hold for all densities relevant to NSs. This may not be always true for ELFc. To stay physical, we switch from ELFc to an expression for the stiffest possible EOS whenever causality is violated:

$$P_{\rm Stiffest}(\mathcal{E}, v_s, \mathcal{E}_0, P_0) = \left(\frac{v_s}{c}\right)^2 (\mathcal{E} - \mathcal{E}_0) + P_0. \tag{14}$$

This equation represents an EOS with constant speed of sound, v_s, and $v_s = c$ yields the stiffest possible EOS [46]. Here $\mathcal{E}_0$ and P_0 are reference values of energy density and pressure, respectively. The reference values can be adjusted to match the conditions at a specific density where energy density and pressure are known. The switch in EOS avoids superfluous rejection when causality is considered.

D. Structure of a NS and modifications on the nuclear EOS

Neutron stars are more than a "giant nucleus" described in Ref. [47]. There are structural changes at various density regions as a result of a competition between the nuclear attraction and the Coulomb repulsion. The dynamics of the outermost layers of NSs is described mostly by the Coulomb repulsion and nuclear masses, where nuclei arrange themselves in a crystalline lattice. As the density increases, it becomes energetically favorable for the electrons to capture protons, and the nuclear system evolves into a Coulomb lattice of progressively more exotic, neutron-rich nuclei that are embedded in a uniform electron gas. This outer crustal region exists as a solid layer of about 1 km in thickness [17].

At intermediate densities of subsaturation, the spherical nuclei that form the crystalline lattice start to deform to reduce the Coulomb repulsion. As a result, the system exhibits rich and complex structures that emerge from a dynamical competition between the short-range nuclear attraction and the long-range Coulomb repulsion [48].

At densities of about half of the nuclear saturation, the uniformity in the system is restored and matter behaves as a uniform Fermi liquid of nucleons and leptons. The transition region from the highly ordered crystal to the uniform liquid core is very complex and not well understood. At these regions of the inner crust which extend about 100 m, various topological structures are thought to emerge that are collectively referred to as "nuclear pasta." Despite the undeniable progress [49–80] in understanding the nuclear-pasta phase since their initial prediction over several decades ago [81–83], there is no known theoretical framework that simultaneously incorporates both quantum-mechanical effects and dynamical correlations beyond the mean-field level. As a result, a reliable EOS for the inner crust is still missing.

The matter in the core region of NSs can be described as uniform nuclear matter where neutrons, protons, electrons, and muons exist in β equilibrium [48]. Although a phase change and exotic matter such as hyperons [48,84,85] could appear in the inner core region, there is currently no direct evidence of their existence. In this work, we calculate the EOS in this region by assuming that the neutron-star matter is composed of nucleons and leptons only.

Due to the rich structure of NSs, the nuclear EOS needs to be contextualized before it can be used for NS properties calculation. To begin with, a crustal EOS should be used at density below the transition density ρ_T. Normally the determination of ρ_T requires complicated thermodynamic calculations, but some simple relationship has been found between transition densities and Taylor parameters of the EOS in Ref. [86] that greatly simplifies its calculation. In this study, the following equation is used to determine ρ_T:

$$\rho_T = (-3.75 \times 10^{-4} L_{\rm sym} + 0.0963)\,{\rm fm}^{-3}. \tag{15}$$

Outer and inner crust exhibit different physical properties and should be described by different EOSs. For the outer crust, the EOS provided by Ref. [87] is used in this analysis. For the inner crust, spline interpolation in the region of $0.3\rho_T < \rho < \rho_T$ is reserved for a smooth transition between the outer crust and outer core. While this connection region cannot precisely describe crustal dynamics, tidal deformability does not appear to be sensitive to the choice of the crustal details for NSs [17,88,89].

The outer core region $\rho > \rho_T$ is characterized by the EOS of a β-equilibrated system of protons, neutrons, electrons, and muons. Protons and neutrons are collectively described by ELFc while electrons and muons are modeled as relativistic Fermi gases. Equilibrium is attained by minimizing the Helmholtz free energy at different densities. If the speed of sound for the EOS reaches the speed of light at density $\rho = \rho_c$, it will switch to the stiffest possible EOS of Eq. (14) at higher densities to comply with the causality condition. If ELFc does not violate causality at all densities relevant to NSs, then $\rho_c = \infty$ and Eq. (14) is never used.

To summarize, the EOS of the neutron-star matter is formulated as follows:

$$P(\mathcal{E}) = \begin{cases} P_{\rm crust}(\mathcal{E}) & \text{if } 0 < \rho < 0.3\rho_T \\ P_{\rm spline}(\mathcal{E}) & \text{if } 0.3\rho_T < \rho < \rho_T \\ P_{\rm ELFc}(\mathcal{E}) & \text{if } \rho_T < \rho < \rho_c \\ P_{\rm stiffest}(\mathcal{E}, c, \mathcal{E}_0, P_0) & \text{if } \rho_c < \rho. \end{cases} \tag{16}$$

In the above equations, $\mathcal{E}_0$ and P_0 are the energy density and pressure from β-equilibrated ELFc at ρ_c, respectively; $P_{\rm crust}$

TABLE I. Summary information of various models [32]. The bottom half shows characteristics of the prior and posterior distribution, respectively.

	$L_{\rm sym}$ (MeV)	$K_{\rm sym}$ (MeV)	$K_{\rm sat}$ (MeV)	$Q_{\rm sym}$ (MeV)	$Q_{\rm sat}$ (MeV)	$Z_{\rm sym}$ (MeV)	$Z_{\rm sat}$ (MeV)	$\frac{m^*_{\rm sat}}{m}$	κ_v
Skyrme average	49.6	−132	237	370	−349	−2175	1448	0.77	0.44
Skyrme σ	21.6	89	27	188	89	1069	510	0.14	0.37
RMF average	90.2	−5	268	271	−2	−3672	5058	0.67	0.40
RMF σ	29.6	88	34	357	393	1582	2294	0.02	0.06
RHF average	90.0	128	248	523	389	−9956	5269	0.74	0.34
RHF σ	11.1	51	12	237	350	4156	838	0.03	0.07
Weighted average	69.0	−45.3	248	367	−114	−3990	3310	0.712	0.42
Weighted σ	20.1	70.8	18.3	214	200	1530	989	0.06	0.17
Posterior average	71.6	−76.9	245	436	−97	−3410	3490	0.74	0.41
Posterior σ	16.5	66.0	23	219	202	1710	970	0.07	0.25

is the pressure from the crustal EOS; and $P_{\rm ELFc}$ is the pressure from the β-equilibrated ELFc EOS. $P_{\rm spline}$ and $\mathcal{E}_{\rm crust}$ govern the cubic spline that smoothly connects $P_{\rm crust}$ to $P_{\rm ELFc}$ and $\mathcal{E}_{\rm crust}$ to $\mathcal{E}_{\rm ELFc}$, respectively.

IV. RESULTS FOR A 1.4-SOLAR-MASS NS

A total of 1 500 000 EOSs have been sampled and 682 652 of them satisfy all of our constraints. Only 11 711 EOSs apply to all densities without switching to the stiffest EOS.

Prior distributions of the parameters should reflect our initial belief of those quantities before information on tidal deformability is taken into account. For this, we rely on Ref. [32] which summarizes the distributions of EOS parameters from three phenomenological families: Skyrme, relativistic mean field (RMF), and relativistic Hartree-Fock (RHF). The mean and standard deviation of the parameters for each family are tabulated in the first six rows of Table I. In this study, the prior means and standard deviations are the weighted average values of the three families, with weights of 0.500, 0.333, and 0.167, respectively. The weights reflect our confidence in the models. We give the Skyrme EOS the most weight as it is the most heavily employed parametrization in a myriad of nuclear predictions [29]. These relative weights are *ad hoc*, but should cover most plausible parameter spaces. Prior means and standard deviations are listed in the seventh and eighth rows in Table I, respectively.

The posterior distributions of Taylor expansion parameters are represented in Fig. 1. The lower triangular plots show the bivariate distributions for two parameters. The diagonal plots show the prior (blue curves) and marginalized posterior distributions (red curves) for individual parameters. The upper triangle displays the Pearson correlation coefficients for parameter pairs:

$$\rho_{X,Y} = \frac{\mathbf{E}[(X-\bar{X})(Y-\bar{Y})]}{\sigma_X \sigma_Y}, \tag{17}$$

where $\mathbf{E}$ is the expectation value and σ_X and σ_Y are the standard deviations of the parameters distributions. The Pearson coefficient ranges from −1 to 1 and its absolute value reflects the strength of the correlation. A positive value close to 1 indicates a strong correlation and a negative value close to −1 indicates strong anticorrelation while a value close to zero indicates lack of correlation [90]. Only bivariate distributions between $L_{\rm sym}$, $K_{\rm sym}$, $K_{\rm sat}$, $Z_{\rm sym}$, and $Z_{\rm sat}$ are shown because the higher order parameters do not seem to be influenced by our tidal deformability constraints. The full correlation plot is included in Appendix C. Characteristics of the probability distribution are summarized in the bottom two rows of Table I.

Figure 2 shows the mean and 2σ region spanned by the EOS in the posterior. The 2σ region converges to a line for $\mathcal{E} \lesssim 20\,{\rm MeV/fm^3}$, which corresponds to the outer crust. Since we connect all EOSs to the crustal EOS given by Ref. [87], this convergence is expected. From around 20 to $70\,{\rm MeV/fm^3}$, the spline connection kicks in and manifests in the broadening of pressure.

The cutoffs in the lower left corner of the $Z_{\rm sym}$ vs $Z_{\rm sat}$ distribution and the upper left corner of the $K_{\rm sym}$ vs $L_{\rm sym}$ distribution in Fig. 1 are the consequence of the stability condition. At such extreme values, the speed of sound may be imaginary when extrapolating to a NS of 2 solar masses. This is evident in Fig. 3 in which 50 randomly selected EOSs from the cutoff region in $K_{\rm sym}$ vs $L_{\rm sym}$ are shown in the lower panel. The pressure for those EOSs does not increase monotonically with the energy density and becomes mechanically unstable. These EOSs are discarded.

The posterior distributions of $K_{\rm sym}$ and $Z_{\rm sym}$ differ from the prior distributions significantly. The tidal deformability constraint favors the lower $K_{\rm sym}$ region. The inference also narrows the range of possible $L_{\rm sym}$. Parameters such as $K_{\rm sat}$ and $Z_{\rm sat}$, whose posterior distributions are not altered significantly, reflect that they are not sensitive to the tidal deformability constraints.

While this Bayesian analysis is well suited to discuss the sensitivity of the deformability to the Taylor expansion parameters $L_{\rm sym}$, $K_{\rm sym}$, $K_{\rm sat}$, etc., it has some limitations. In particular, we note that the prior and post distributions of Λ as shown in Fig. 7 (row 2, column 10,) are drastically different, probably as a consequence of the narrow prior distributions of the Taylor expansion parameters listed in Table I. This reflects the strong sensitivity of Λ to the prior distributions of the EOS. Furthermore, the posterior distribution of Λ is much sharper and peaked at 624 ± 129 which exceeds the value of 190^{+390}_{-120} obtained in Ref. [18] from the analysis of the

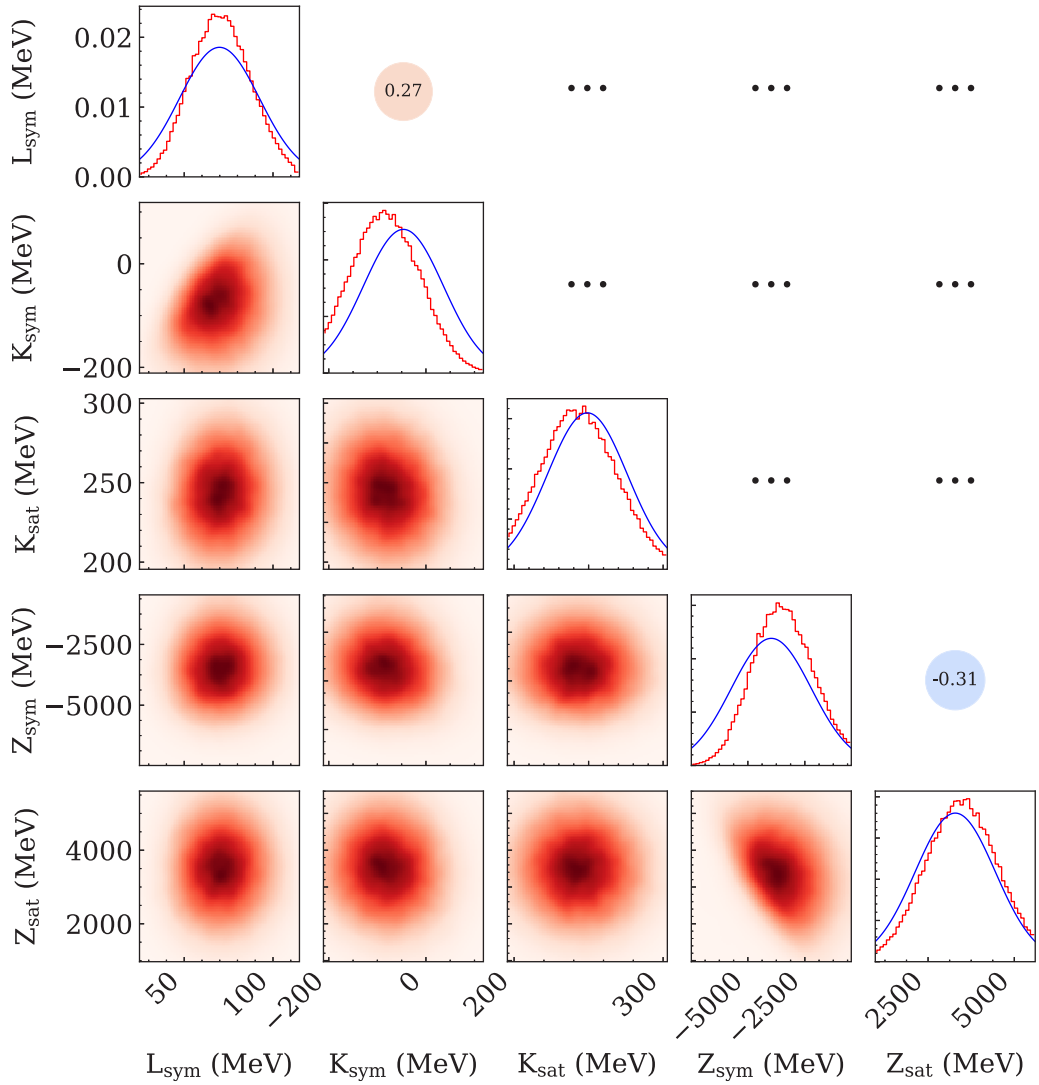

FIG. 1. Bivariate characteristics of posterior likelihood distributions. Three regions can be distinguished. The lower triangle panels show likelihood distributions, with intensity proportional to distribution value, for pairs of Taylor parameters. The diagonal panels display prior (blue) and marginalized posterior (red) distributions for each parameter. The upper triangular region shows the Pearson correlation coefficient for parameter pairs. Three dots indicate weak correlations with magnitude less than 0.1.

GW170817. While the GW constraint reflects the high density of the NS core, the prior distributions of the Taylor expansion parameters do not have rigorous laboratory constraints at the high density region where Λ is determined.

V. NEUTRON STAR WITH DIFFERENT MASSES

While the chirp mass of GW170817 has been determined quite accurately [11], the exact masses of the two neutron stars or their mass ratios are not known [11]. In anticipation that more merger events involving different NS masses than the nominal NS mass of 1.4 solar masses are observed in the future [91], we use the posterior EOS distributions to predict the deformability of a NS with different masses. The posterior EOS distributions can be used to predict the deformability of a NS with different masses. In Table II, we provide our predictions for the tidal deformabilities for a NS with 1.2, 1.4, 1.6, 1.8, and 2 solar masses using this group of EOSs weighted by their posterior distributions. To show the sensitivity of these predictions to the Taylor parameters, Fig. 4 shows the bivariate distributions between the Taylor parameters of the posterior distributions and the predicted tidal deformabilities of different stellar masses. We find that Λ is more strongly correlated with L_{sym} and K_{sym} than it is with higher order Taylor expansion parameters. The sensitivity to K_{sym} increases, while the sensitivity to L_{sym} decreases, with stellar mass.

To quantify this dependence of sensitivity on mass, the Pearson correlation coefficients for a few selected Taylor

TABLE II. Predicted tidal deformability for NSs of different masses.

	$\Lambda(1.2)$	$\Lambda(1.4)$	$\Lambda(1.6)$	$\Lambda(1.8)$	$\Lambda(2.0)$
Posterior average	1490	624	281	132	64
Posterior σ	310	129	61	31	17

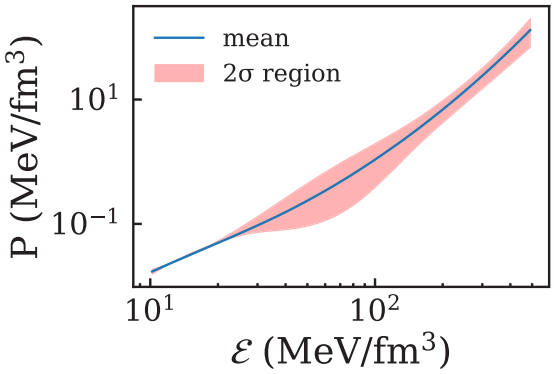

FIG. 2. Distribution of EOSs sampled from the posterior. The divergence above energy density $\gtrsim$20 MeV/fm^3 coincides with the transition from outer crust to spline connection.

parameter pairs are shown in Fig. 5. A gradual reduction in correlation between $L_{\rm sym}$ and tidal deformability is observed as the mass of a NS increases. This is expected as the relevant average density for more massive stars shifts upward and away from those most directly impacted by $L_{\rm sym}$. A high density parameter $P(2\rho_0)$, the pressure for pure neutron matter at twice the saturation density, is also included in Figs. 4 and 5. The strong correlation between tidal deformability and $P(2\rho_0)$

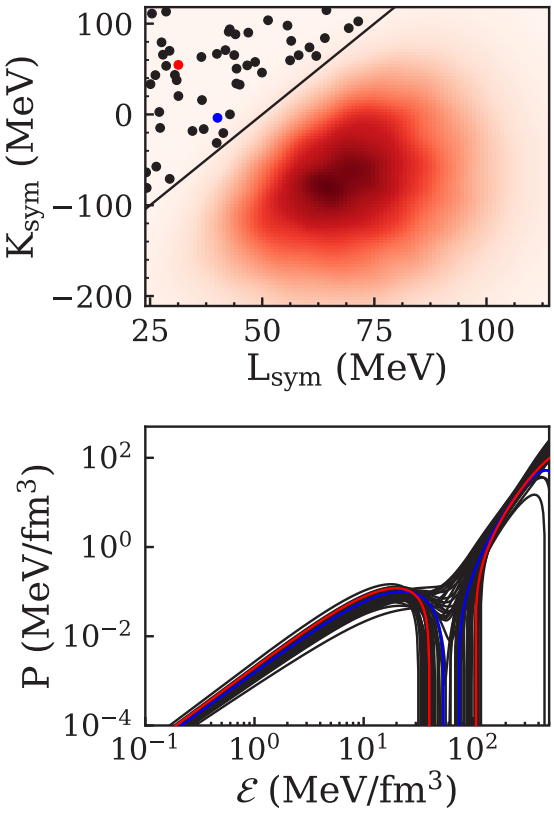

FIG. 3. Top: The 50 dots in the upper left hand corner of $K_{\rm sym}$ vs $L_{\rm sym}$ correspond to 50 randomly chosen parameter spaces within the stability cutoff region. Bottom: Unstable EOS corresponding to the 50 dots. The red and blue lines correspond to the red and blue points in the upper panel, respectively. They are highlighted to showcase what a typical EOS in the cutoff region looks like.

is consistent with prior work [18,27,28,92]. While this strong correlation is maintained for both heavy and light NSs, the slope of the correlation becomes smaller, reflecting the decrease in average values and variations of Λ with stellar mass.

Such a decrease is correlated with an increase in stellar compactness. Using the posterior probability distributions for the Taylor expansion parameters, we can also make predictions on the relation between stellar mass and inverse compactness (R/M). Figure 6 shows tidal deformability plotted against inverse compactness, with calculation results for 1.2-, 1.4-, 1.6-, and 1.8-solar-mass NSs all combined together. It is consistent with Eq. (2) where $\Lambda \propto k_2 (R/M)^5$. The best fitted power law has an index of 5.84 due to additional interdependence of tidal Love number k_2 and R/M. The result is consistent with Refs. [17,93,94].

Recently, we found that, independently and in parallel, Ref. [44] conducted a very similar analysis using ELFc. Our work examines correlations between more parameters and our study extends to a higher mass neutron star. Reference [44] uses much wider priors while our prior is more restrictive and provides finer details in a smaller phase space. In addition, they apply additional constraints on the EOS using data from the Chiral effective field theory (χEFT) approach and isoscalar giant monopole resonance (ISGMR) collective mode. Even though their extracted $Q_{\rm sat}$ and $K_{\rm sym}$ values are consistent with our extracted values, details in the correlations are not the same. The subtle differences suggest that Bayesian analysis results depend on the choice of priors and constraints applied to the EOS.

VI. CONCLUSION

In this paper, the ELFc form of metamodeling is used in a sensitivity study of NS tidal deformability to Taylor expansion parameters of the nuclear equation of state. Constraints on the isoscalar parameters, such as $K_{\rm sat}$, are found to be less affected by NS properties. For the isovector parameters, $L_{\rm sym}$ is found to be most correlated with tidal deformability, closely followed by $K_{\rm sym}$, although the importance of the former dwindles and reverses as NS mass increases to above 1.6 solar masses.

We have further demonstrated the global relation between tidal deformability and compactness of NSs with different masses. When more merger events involving different NS masses are observed in the future, one can verify the relation of tidal deformability and inverse compactness in Fig. 6 and provide independent constraints on $L_{\rm sym}$ and $K_{\rm sym}$.

A strong correlation with the pressure of matter at $2\rho_0$ is observed. This highlights the need for high density observables from nuclear physics, as constraints on tidal deformability can be tightened with accurate high density observations. A strong experimental constraint on pressure for PNM at $2\rho_0$ complements pressure [95,96] constraints from future measurement of NS mergers.

ACKNOWLEDGMENTS

This work was partly supported by the US National Science Foundation under Grant No. PHY-1565546 and by

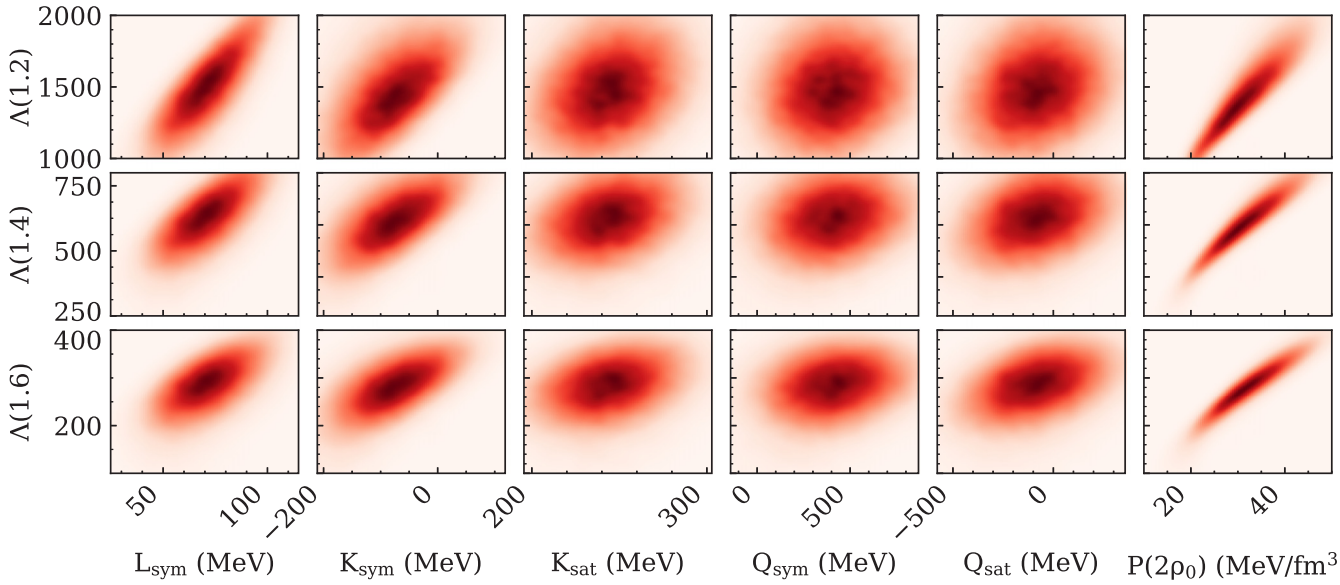

FIG. 4. Bivariate distributions between deformabilities with NSs of different masses and Taylor parameters. Correlation with tidal deformability is clearly seen with $L_{\rm sym}$, $K_{\rm sym}$, and $P(2\rho_0)$.

the US Department of Energy (Office of Science) under Grants No. DE-SC0014530, No. DE-NA0002923, and No. DE-SC001920. All the NS model calculations with high performance computers were performed at the Institute for Cyber Enabled Research at Michigan State University.

APPENDIX A: TOV EQUATION

The TOV equation set predicts the structure of a static spherical object under general relativity for any given EOS. The equations are

$$\frac{dP(r)}{dr} = -\frac{(\mathcal{E}(r)+P(r))(M(r)+4\pi r^3 P(r))}{r^2(1-2M(r)/r)},$$
$$\frac{dM(r)}{dr} = 4\pi r^2 \mathcal{E}(r). \tag{A1}$$

Here geometrized units $G = c = 1$ are used, $\mathcal{E}(r)$ is the energy density given by the EOS, $P(r)$ is the internal pressure at given depth, and $M(r)$ is the integral of gravitational mass from the core up to radius r. The surface is defined as the radial distance R at which $P(R) = 0$.

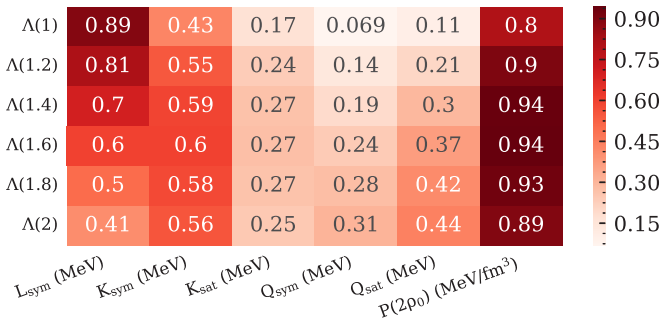

FIG. 5. Pearson correlation parameters for different NS masses.

A list of equations whose solutions lead to the value of Λ from the above structural functions is shown without derivation. Please refer to Refs. [16,97] for details. To begin with, an auxiliary variable $y_R = y(R)$ is calculated,

$$r\frac{dy(r)}{dr} + y(r)^2 + y(r)F(r) + r^2 Q(r) = 0, \tag{A2}$$

where

$$F(r) = \frac{r - 4\pi r^3(\mathcal{E}(r) - P(r))}{r - 2M(r)}, \tag{A3}$$

$$Q(r) = \frac{4\pi r(5\mathcal{E}(r) + 9P(r) + \frac{\mathcal{E}+P(r)}{\partial P(r)/\partial \mathcal{E}} - \frac{6}{4\pi r^2}}{r - 2M(r)} - 4\left[\frac{(M(r) + 4\pi r^3 P(r)}{r^2(1-2M(r)/r)}\right]^2. \tag{A4}$$

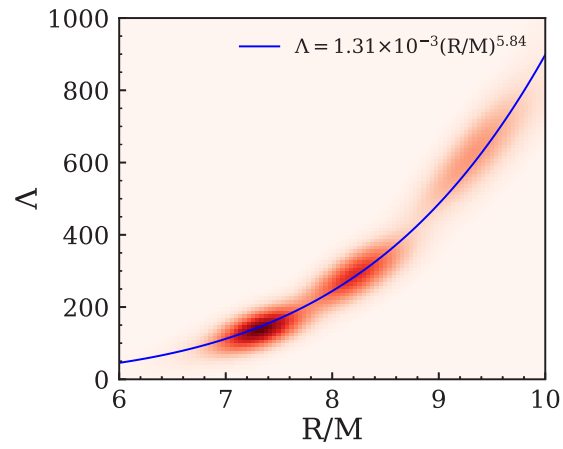

FIG. 6. Tidal deformability vs inverse compactness for 1.2-, 1.4-, 1.6-, and 1.8-solar-mass NS.

The tidal Love number k_2 can then be calculated with the following expression:

$$k_2 = \frac{1}{20}\left(\frac{R_s}{R}\right)^5\left(1-\frac{R_s}{R}\right)^2\left[2-y_R+(y_R-1)\frac{R_s}{R}\right]\left\{\frac{R_s}{R}\left(6-3y_R+\frac{3R_s}{2R}(5y_R-8)+\frac{1}{4}\left(\frac{R_s}{R}\right)^2\right.\right.$$
$$\left.\left.\times\left[26-22y_R+\frac{R_s(3y_R-2)}{R}+\left(\frac{R_S}{R}\right)^2(1+y_R)\right]\right)+3\left(1-\frac{R_s}{R}\right)^2\left[2-y_R+\frac{R_s(y_R-1)}{R}\right]\ln\left(1-\frac{R_S}{R}\right)\right\}^{-1}. \quad \text{(A5)}$$

In the above, $R_S = 2M$ is the Schwarzschild radius. The value of Λ is then extracted with Eq. (2).

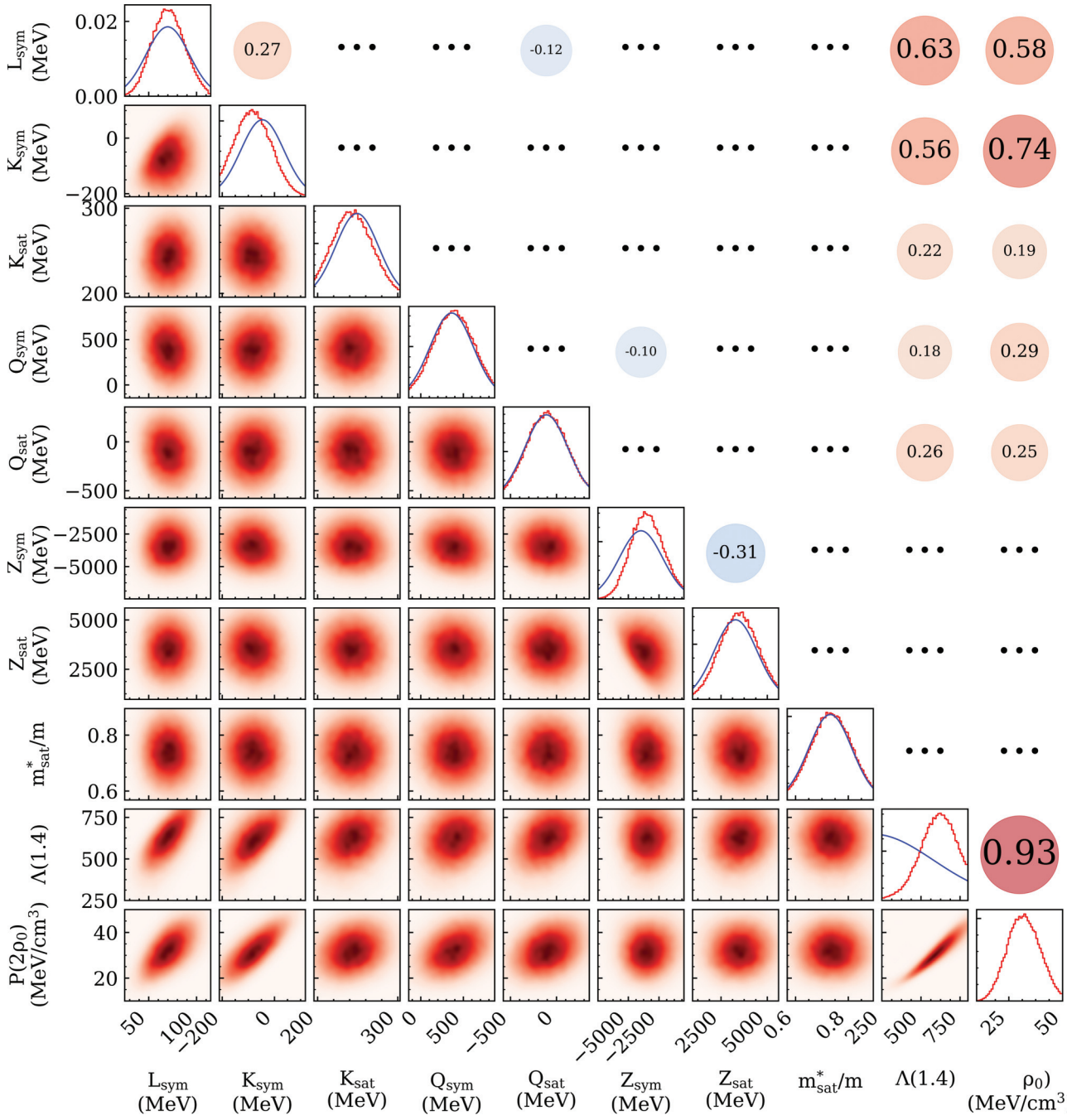

FIG. 7. Bivariate characteristics of posterior likelihood distributions. This is an extension of Fig. 1 and correlation pairs of all parameters are shown. Three regions can be distinguished. The lower triangle panels show likelihood distributions, with intensity proportional to distribution value, for pairs of Taylor parameters. The diagonal panels display the marginalized distribution for each parameter. The upper triangular region shows Pearson correlation coefficients for parameter pairs, but when correlation in magnitude is less than 0.1, it is omitted and three dots are put in place of its value.

APPENDIX B: METAMODELING PARAMETERS AND TAYLOR PARAMETERS MAPPING

The ELFc energy functional is written as a sum of kinetic energy and potential energy terms:

$$E_{\mathrm{EFLc}}(\rho,\delta) = t^{FG*}(\rho,\delta) + v^{N}_{\mathrm{EFLc}}(\rho,\delta), \tag{B1}$$

where ρ is the density and δ is the asymmetry parameter. The kinetic energy term $t^{FG*}(\rho,\delta)$ in the above is written as

$$t^{FG*}(\rho,\delta) = \frac{t^{FG}_{\mathrm{sat}}}{2}\left(\frac{\rho}{\rho_0}\right)^{\frac{2}{3}}\left[\left(1+\frac{\kappa_{\mathrm{sat}}\rho}{\rho_0}\right)\left((1+\delta)^{\frac{5}{3}}+(1-\delta)^{\frac{5}{3}}\right) + \frac{\kappa_{\mathrm{sym}}\rho}{\rho_0}\delta\left((1+\delta)^{\frac{5}{3}}-(1-\delta)^{\frac{5}{3}}\right)\right]. \tag{B2}$$

In the above, the parameter $t^{FG}_{\mathrm{sat}} = 22.1\,\mathrm{MeV}$ while κ_{sym} and κ_{sat} are effective mass parameters described in Eq. (11).

The potential energy term $v^{N}_{\mathrm{EFLc}}(\rho,\delta)$ is written as

$$v^{N}_{\mathrm{EFLc}}(\rho,\delta) = \sum_{i=0}^{4}\frac{1}{i!}\left(v_i^{is}+v_i^{iv}\delta^2\right)\left(1-(-3)^{5-i}\right) \times \exp\left(-\frac{6.93\rho}{\rho_0}\right)x^i. \tag{B3}$$

In the above, the parameters v_i^{is} and v_i^{iv} are free parameters. These ten parameters can be uniquely mapped onto Taylor parameters using the following formulas (for a detailed derivation, please refer to Ref. [32]):

$$v_0^{is} = E_{\mathrm{sat}} - t^{FG}_{\mathrm{sat}}(1+\kappa_{\mathrm{sat}}), \tag{B4}$$

$$v_1^{is} = -t^{FG}_{\mathrm{sat}}(2+5\kappa_{\mathrm{sat}}), \tag{B5}$$

$$v_2^{is} = K_{\mathrm{sat}} - 2t^{FG}_{\mathrm{sat}}(-1+5\kappa_{\mathrm{sat}}), \tag{B6}$$

$$v_3^{is} = Q_{\mathrm{sat}} - 2t^{FG}_{\mathrm{sat}}(4-5\kappa_{\mathrm{sat}}), \tag{B7}$$

$$v_4^{is} = Z_{\mathrm{sat}} - 8t^{FG}_{\mathrm{sat}}(-7+5\kappa_{\mathrm{sat}}), \tag{B8}$$

$$v_0^{iv} = S_0 - \frac{5}{9}t^{FG}_{\mathrm{sat}}(1+(\kappa_{\mathrm{sat}}+3\kappa_{\mathrm{sym}})), \tag{B9}$$

$$v_1^{iv} = L - \frac{5}{9}t^{FG}_{\mathrm{sat}}(2+5(\kappa_{\mathrm{sat}}+3\kappa_{\mathrm{sym}})), \tag{B10}$$

$$v_2^{iv} = K_{\mathrm{sym}} - \frac{10}{9}t^{FG}_{\mathrm{sat}}(-1+5(\kappa_{\mathrm{sat}}+3\kappa_{\mathrm{sym}})), \tag{B11}$$

$$v_3^{iv} = Q_{\mathrm{sym}} - \frac{10}{9}t^{FG}_{\mathrm{sat}}(4-5(\kappa_{\mathrm{sat}}+3\kappa_{\mathrm{sym}})), \tag{B12}$$

$$v_4^{iv} = Z_{\mathrm{sym}} - \frac{40}{9}t^{FG}_{\mathrm{sat}}(-7+5(\kappa_{\mathrm{sat}}+3\kappa_{\mathrm{sym}})). \tag{B13}$$

When exploring the parameter space, Taylor parameters will be translated to a metamodeling EOS using the above formulas and NS features will then be calculated with the TOV equation. Neutron star properties will be examined in order to search for Taylor parameter spaces flavored by the observed tidal deformability.

APPENDIX C: FULL CORRELATION BETWEEN TIDAL DEFORMABILITY AND PARAMETERS

The correlation between L_{sym}, K_{sym}, K_{sat}, Q_{sym}, Q_{sat}, Z_{sym}, Z_{sat}, (m_{sat}/m), $P(2\rho_0)$, and Λ are shown in Fig. 7. This is an extension of Fig. 4 where bivariate distributions of some selected parameters are shown. The organization is similar: Lower triangles show bivariate distributions between variables and marginal distribution of each variable is shown on the diagonal. The upper triangles show Pearson correlation coefficients between each variable pair if it is larger than 0.1; otherwise they are omitted for simplicity and three dots are put in their place.

[1] B.-A. Li, P. G. Krastev, D.-H. Wen, and N.-B. Zhang, Eur. Phys. J. A **55**, 117 (2019).
[2] M. Baldo and G. Burgio, Prog. Part. Nucl. Phys. **91**, 203 (2016).
[3] J. M. Lattimer, Annu. Rev. Nucl. Part. Sci. **62**, 485 (2012).
[4] J. W. Holt and N. Kaiser, Phys. Rev. C **95**, 034326 (2017).
[5] M. Tsang, W. Lynch, P. Danielewicz, and C. Tsang, Phys. Lett. B **795**, 533 (2019).
[6] P. Danielewicz, R. Lacey, and W. G. Lynch, Science **298**, 1592 (2002).
[7] C. Fuchs, Prog. Part. Nucl. Phys. **56**, 1 (2006).
[8] W. G. Lynch, M. B. Tsang, Y. Zhang, P. Danielewicz, M. Famiano, Z. Li, and A. W. Steiner, Prog. Part. Nucl. Phys. **62**, 427 (2009).
[9] A. L. Fèvre, Y. Leifels, W. Reisdorf, J. Aichelin, and C. Hartnack, Nucl. Phys. A **945**, 112 (2016).
[10] A. W. Steiner, J. M. Lattimer, and E. F. Brown, Astrophys. J. **765**, L5 (2013).
[11] B. P. Abbott *et al.* (LIGO Scientific Collaboration and Virgo Collaboration), Phys. Rev. Lett. **119**, 161101 (2017).
[12] T. Damour, M. Soffel, and C. Xu, Phys. Rev. D **45**, 1017 (1992).
[13] E. E. Flanagan and T. Hinderer, Phys. Rev. D **77**, 021502(R) (2008).
[14] T. Damour, A. Nagar, and L. Villain, Phys. Rev. D **85**, 123007 (2012).
[15] T. Binnington and E. Poisson, Phys. Rev. D **80**, 084018 (2009).
[16] S. Postnikov, M. Prakash, and J. M. Lattimer, Phys. Rev. D **82**, 024016 (2010).
[17] J. Piekarewicz and F. J. Fattoyev, Phys. Rev. C **99**, 045802 (2019).
[18] B. P. Abbott *et al.* (LIGO Scientific Collaboration and Virgo Collaboration), Phys. Rev. Lett. **121**, 161101 (2018).
[19] M. Kortelainen, T. Lesinski, J. Moré, W. Nazarewicz, J. Sarich, N. Schunck, M. V. Stoitsov, and S. Wild, Phys. Rev. C **82**, 024313 (2010).
[20] B. A. Brown, Phys. Rev. Lett. **111**, 232502 (2013).
[21] Z. Zhang and L.-W. Chen, Phys. Lett. B **726**, 234 (2013).
[22] P. Danielewicz, P. Singh, and J. Lee, Nucl. Phys. A **958**, 147 (2017).
[23] C. Y. Tsang, M. B. Tsang, P. Danielewicz, F. J. Fattoyev, and W. G. Lynch, Phys. Lett. B **796**, 1 (2019).

[24] T. Malik, N. Alam, M. Fortin, C. Providência, B. K. Agrawal, T. K. Jha, B. Kumar, and S. K. Patra, Phys. Rev. C **98**, 035804 (2018).
[25] H. Gil, Y.-M. Kim, C. H. Hyun, P. Papakonstantinou, and Y. Oh, Phys. Rev. C **100**, 014312 (2019).
[26] Z. Carson, A. W. Steiner, and K. Yagi, Phys. Rev. D **99**, 043010 (2019).
[27] Y. Lim and J. W. Holt, Phys. Rev. Lett. **121**, 062701 (2018).
[28] J. M. Lattimer and M. Prakash, Astrophys. J. **550**, 426 (2001).
[29] M. Dutra, O. Lourenço, J. S. Sá Martins, A. Delfino, J. R. Stone, and P. D. Stevenson, Phys. Rev. C **85**, 035201 (2012).
[30] E. Khan, J. Margueron, and I. Vidaña, Phys. Rev. Lett. **109**, 092501 (2012).
[31] E. Khan, Phys. Scr. **T152**, 014008 (2013).
[32] J. Margueron, R. Hoffmann Casali, and F. Gulminelli, Phys. Rev. C **97**, 025805 (2018).
[33] P. Demorest, T. Pennucci, S. Ransom, M. Roberts, and J. Hessels, Nature **467**, 1081 (2010).
[34] J. Antoniadis, P. C. C. Freire, N. Wex, T. M. Tauris, R. S. Lynch, M. H. van Kerkwijk, M. Kramer, C. Bassa, V. S. Dhillon, T. Driebe, J. W. T. Hessels, V. M. Kaspi, V. I. Kondratiev, N. Langer, T. R. Marsh, M. A. McLaughlin, T. T. Pennucci, S. M. Ransom, I. H. Stairs, J. van Leeuwen, J. P. W. Verbiest, and D. G. Whelan, Science **340**, 1233232 (2013).
[35] B. Margalit and B. D. Metzger, Astrophys. J. **850**, L19 (2017).
[36] G. Baym, S. Furusawa, T. Hatsuda, T. Kojo, and H. Togashi, Astrophys. J. **885**, 42 (2019).
[37] B.-A. Li, P. G. Krastev, D.-H. Wen, W.-J. Xie, and N.-B. Zhang, AIP Conf. Proc. **2127**, 020018 (2019).
[38] M. Shibata, S. Fujibayashi, K. Hotokezaka, K. Kiuchi, K. Kyutoku, Y. Sekiguchi, and M. Tanaka, Phys. Rev. D **96**, 123012 (2017).
[39] L. Rezzolla, E. R. Most, and L. R. Weih, Astrophys. J. **852**, L25 (2018).
[40] M. Ruiz, S. L. Shapiro, and A. Tsokaros, Phys. Rev. D **97**, 021501(R) (2018).
[41] E.-P. Zhou, X. Zhou, and A. Li, Phys. Rev. D **97**, 083015 (2018).
[42] E. Lipparini and S. Stringari, Phys. Rep. **175**, 103 (1989).
[43] I. Tews, J. Margueron, and S. Reddy, Phys. Rev. C **98**, 045804 (2018).
[44] H. Guven, K. Bozkurt, E. Khan, and J. Margueron, Phys. Rev. C **102**, 015805 (2020).
[45] L. D. Landau and E. M. Lifshitz, *Fluid Mechanics* (Pergamon, Oxford, 1987), pp. 251–254.
[46] J. M. Lattimer and M. Prakash, Phys. Rep. **621**, 127 (2016).
[47] D. G. Yakovlev, P. Haensel, G. Baym, and C. Pethick, Phys. Usp. **56**, 289 (2013).
[48] P. Haensel, A. Y. Potekhin, and D. G. Yakovlev, *Neutron Stars I* (Springer, Berlin, 2007).
[49] K. Nakazato, K. Iida, and K. Oyamatsu, Phys. Rev. C **83**, 065811 (2011).
[50] F. Sébille, V. de la Mota, and S. Figerou, Phys. Rev. C **84**, 055801 (2011).
[51] K. Vantournhout, T. Neff, H. Feldmeier, N. Jachowicz, and J. Ryckebusch, Prog. Part. Nucl. Phys. **66**, 271 (2011).
[52] H. Pais and J. R. Stone, Phys. Rev. Lett. **109**, 151101 (2012).
[53] N. Gupta and P. Arumugam, Phys. Rev. C **87**, 028801 (2013).
[54] M. Okamoto, T. Maruyama, K. Yabana, and T. Tatsumi, Phys. Rev. C **88**, 025801 (2013).
[55] P. N. Alcain, P. A. Giménez Molinelli, J. I. Nichols, and C. O. Dorso, Phys. Rev. C **89**, 055801 (2014).
[56] F. Grill, H. Pais, C. Providência, I. Vidaña, and S. S. Avancini, Phys. Rev. C **90**, 045803 (2014).
[57] N. Martin and M. Urban, Phys. Rev. C **92**, 015803 (2015).
[58] P. G. Molinelli and C. Dorso, Nucl. Phys. A **933**, 306 (2015).
[59] I. Sagert, G. I. Fann, F. J. Fattoyev, S. Postnikov, and C. J. Horowitz, Phys. Rev. C **93**, 055801 (2016).
[60] R. Nandi and S. Schramm, Phys. Rev. C **94**, 025806 (2016).
[61] S. Kubis and W. Wójcik, Phys. Rev. C **94**, 065805 (2016).
[62] G. Grams, A. M. Santos, P. K. Panda, C. Providência, and D. P. Menezes, Phys. Rev. C **95**, 055807 (2017).
[63] R. A. Kycia, S. Kubis, and W. Wójcik, Phys. Rev. C **96**, 025803 (2017).
[64] B. Schuetrumpf, G. Martínez-Pinedo, M. Afibuzzaman, and H. M. Aktulga, Phys. Rev. C **100**, 045806 (2019).
[65] J. M. Pearson, N. Chamel, and A. Y. Potekhin, Phys. Rev. C **101**, 015802 (2020).
[66] C. C. Barros, D. P. Menezes, and F. Gulminelli, Phys. Rev. C **101**, 035211 (2020).
[67] C. J. Horowitz, M. A. Pérez-García, and J. Piekarewicz, Phys. Rev. C **69**, 045804 (2004).
[68] C. J. Horowitz, M. A. Pérez-García, J. Carriere, D. K. Berry, and J. Piekarewicz, Phys. Rev. C **70**, 065806 (2004).
[69] C. J. Horowitz, M. A. Pérez-García, D. K. Berry, and J. Piekarewicz, Phys. Rev. C **72**, 035801 (2005).
[70] G. Watanabe, K. Sato, K. Yasuoka, and T. Ebisuzaki, Phys. Rev. C **68**, 035806 (2003).
[71] G. Watanabe, T. Maruyama, K. Sato, K. Yasuoka, and T. Ebisuzaki, Phys. Rev. Lett. **94**, 031101 (2005).
[72] G. Watanabe, H. Sonoda, T. Maruyama, K. Sato, K. Yasuoka, and T. Ebisuzaki, Phys. Rev. Lett. **103**, 121101 (2009).
[73] A. S. Schneider, C. J. Horowitz, J. Hughto, and D. K. Berry, Phys. Rev. C **88**, 065807 (2013).
[74] C. J. Horowitz, D. K. Berry, C. M. Briggs, M. E. Caplan, A. Cumming, and A. S. Schneider, Phys. Rev. Lett. **114**, 031102 (2015).
[75] M. E. Caplan, A. S. Schneider, C. J. Horowitz, and D. K. Berry, Phys. Rev. C **91**, 065802 (2015).
[76] P. Magierski and P.-H. Heenen, Phys. Rev. C **65**, 045804 (2002).
[77] N. Chamel, Nucl. Phys. A **747**, 109 (2005).
[78] W. G. Newton and J. R. Stone, Phys. Rev. C **79**, 055801 (2009).
[79] B. Schuetrumpf and W. Nazarewicz, Phys. Rev. C **92**, 045806 (2015).
[80] F. J. Fattoyev, C. J. Horowitz, and B. Schuetrumpf, Phys. Rev. C **95**, 055804 (2017).
[81] D. G. Ravenhall, C. J. Pethick, and J. R. Wilson, Phys. Rev. Lett. **50**, 2066 (1983).
[82] M. Hashimoto, H. Seki, and M. Yamada, Prog. Theor. Phys. **71**, 320 (1984).
[83] K. Oyamatsu, M.-a. Hashimoto, and M. Yamada, Prog. Theor. Phys. **72**, 373 (1984).
[84] V. A. Ambartsumyan and G. S. Saakyan, Sov. Astron. **4**, 187 (1960).
[85] D. Chatterjee and I. Vidaña, Eur. Phys. J. A **52**, 29 (2016).
[86] C. Ducoin, J. Margueron, C. Providência, and I. Vidaña, Phys. Rev. C **83**, 045810 (2011).
[87] G. Baym, C. Pethick, and P. Sutherland, Astrophys. J. **170**, 299 (1971).
[88] F. Ji, J. Hu, S. Bao, and H. Shen, Phys. Rev. C **100**, 045801 (2019).

[89] L. Perot, N. Chamel, and A. Sourie, Phys. Rev. C **101**, 015806 (2020).
[90] J. Benesty, J. Chen, Y. Huang, and I. Cohen, *Noise Reduction in Speech Processing*, Vol. 2 (Springer, Berlin, 2009).
[91] B. P. Abbott *et al.* (LIGO Scientific Collaboration and Virgo Collaboration), Astrophys. J. Lett **892**, L3 (2020).
[92] I. Tews, J. Carlson, S. Gandolfi, and S. Reddy, Astrophys. J. **860**, 149 (2018).
[93] A. Maselli, V. Cardoso, V. Ferrari, L. Gualtieri, and P. Pani, Phys. Rev. D **88**, 023007 (2013).
[94] J. M. Lattimer (private communication).
[95] R. Shane, A. B. McIntosh, T. Isobe, W. G. Lynch, H. Baba, J. Barney, Z. Chajecki, M. Chartier, J. Estee, M. Famiano, B. Hong, K. Ieki, G. Jhang, R. Lemmon, F. Lu, T. Murakami, N. Nakatsuka, M. Nishimura, R. Olsen, W. Powell, H. Sakurai, A. Taketani, S. Tangwancharoen, M. B. Tsang, T. Usukura, R. Wang, S. J. Yennello, and J. Yurkon, Nucl. Instrum. Methods Phys. Res., Sect. A **784**, 513 (2015).
[96] P. Russotto *et al.*, Phys. Rev. C **94**, 034608 (2016).
[97] F. J. Fattoyev, J. Carvajal, W. G. Newton, and B.-A. Li, Phys. Rev. C **87**, 015806 (2013).